Advances in Nano Research, *Vol. 15, No. 4 (2023) 315-328*
https://doi.org/10.12989/anr.2023.15.4.315

Predicting ESP and HNT effects on the mechanical properties of eco-friendly composites subjected to micro-indentation test

Saeed Kamarian*[1], Ali Khalvandi[2,3], Thanh Mai Nguyen Tran[1,4], Reza Barbaz-Isfahani[2,3], Saeed Saber-Samandari[2,3] and Jung-Il Song**[1]

[1]*Department of Mechanical Engineering, Changwon National University, Changwon, South Korea*
[2]*Composites Research Laboratory (CRLab), Amirkabir University of Technology, Tehran, Iran*
[3]*New Technologies Research Center, Amirkabir University of Technology, Tehran, Iran*
[4]*Faculty of civil engineering, Nha Trang University, Nha Trang 650000, Vietnam*

(*Received June 11, 2022, Revised November 25, 2022, Accepted January 26, 2023*)

Abstract. The main goal of the present study was to assess the effects of eggshell powder (ESP) and halloysite nanotubes (HNTs) on the mechanical properties of abaca fiber (AF)-reinforced natural composites. For this purpose, a limited number of indentation tests were first performed on the AF/polypropylene (PP) composites for different HNT and ESP loadings (0 wt.% ~ 6 wt.%), load amplitudes (150, 200, and 250 N), and two types of indenters (Vickers or conical). The Young's modulus, hardness and plasticity index of each specimen were calculated using the indentation test results and Oliver-Pharr method. The accuracy of the experimental results was confirmed by comparing the values of the Young's modulus obtained from the indentation test with the results of the conventional tensile test. Then, a feed-forward shallow artificial neural network (ANN) with high efficiency was trained based on the obtained experimental data. The trained ANN could properly predict the variations of the mentioned mechanical properties of AF/PP composites incorporated with different HNT and ESP loadings. Furthermore, the trained ANN demonstrated that HNTs increase the elastic modulus and hardness of the composite, while the incorporation of ESP reduces these properties. For instance, the Young's modulus of composites incorporated with 3 wt.% of ESP decreased by 30.7% compared with the pure composite, while increasing the weight fraction of ESP up to 6% decreased the Young's modulus by 34.8%. Moreover, the trained ANN indicated that HNTs have a more significant effect on reducing the plasticity index than ESP.

Keywords: abaca fiber; artificial neural network; eco-friendly composites; egg shell powder; halloysite nanotubes; indentation test; polypropylene

1. Introduction

Increasing concerns about environmental pollution and irreparable damage from the use of nondegradable products have encouraged the application of eco-friendly materials in various industries (Kamarian and Song 2022). Natural fibers (NFs) are inexpensive, lightweight, biodegradable, and abundant with wide applications in the manufacturing of composite products in various industries, including automobiles, construction, furniture, and railways.

Among the NFs available in the market, abaca fiber (AF) is a contender for the production of NF composites. The AF originates from a plant called Musa textilis (Ochi 2006). The Philippines is the world's largest producer of abaca, supplying approximately 84% of the global demand, which averages 68,000 t annually (Barba *et al*. 2020). Morphologically, AF resembles a banana plant with 12–30 stems originating from a central root system, giving it a bushy appearance. Each stalk can grow to 4–8 m and these stalks are plucked to form AF. The fibers are usually 1.5–3.5 m in length and have different colors: white, brown, red, black, or purple (Vijayalakshmi *et al*. 2014). AF is one of the strongest NFs available on the market and is currently used in many applications. Owing to its high mechanical strength, durability, flexibility, high resistance to saltwater, buoyancy, and long fiber length, it has great potential as a renewable fiber source for industrial applications. This fiber consists of approximately 60% cellulose, 21% hemicellulose, 12%–16% lignin, and 1% pectin (Sun *et al*. 1998). Its high stiffness and strength are caused by three important microstructural features: a high Runkle ratio (Liu *et al*. 2013), a high ratio of cellulose to hemicellulose and lignin (Vijayalakshmi *et al*. 2014), and a microfibril angle oriented close to the fiber bundle (Madsen and Gamstedt 2013). AF-reinforced composites have been the subject of numerous studies in recent years, and their behavior has been extensively investigated under bending (Vijaya Ramnath *et al*. 2014), tensile (Vasquez and Diaz 2017), compressive (Manickavasagam *et al*. 2014), impact (Shaik and Subramanian 2021, Vijaya Ramnath *et al*. 2014), and thermal (Li *et al*. 2017) loads.

Chicken eggshells are a poultry byproduct and have been listed as one of the worst environmental pollutants worldwide. They comprise a three-layered structure: a

*Corresponding author, Ph.D.,
E-mail: kamarian@changwon.ac.kr
kamarian.saeed@yahoo.com
**Co-corresponding author, Ph.D.,
E-mail: jisong@changwon.ac.kr

ISSN: 2287-237X (Print), 2287-2388 (Online)

cuticle on the outer surface, a spongy layer, and an inner layer (Kang *et al*. 2010). The chemical composition (by weight) of eggshells is reported to be 94% calcium carbonate, 1% magnesium carbonate, 1% calcium phosphate, and 4% organic matter (Tsai *et al*. 2006). Studies have shown that eggshells can replace 75% of commercial $CaCO_3$ and talc as biofillers in polypropylene composites. Furthermore, various efforts have recently been made to reuse eggshells as valuable items, such as environmentally friendly catalysts, advanced materials for bone tissue stabilization, adsorbents of some metal particles, and microporous calcium oxide (Jena and Sahoo 2019, Jirimali *et al*. 2018, Xu *et al*. 2019).

Halloysite nanotubes (HNTs), $Al_2Si_2O_5(OH)_4.2H_2O$, belong to a subgroup of Kaolin clays, which are unique and versatile nanomaterials constituting a double layer of aluminum, silicon, hydrogen, and oxygen. HNTs have a porous structure that has been adopted as a reinforcing agent in plastic composites (Deng *et al*. 2008, Liu *et al*. 2008), as well as biological and medical applications (Massaro *et al*. 2017, Santos *et al*. 2018). Specifically, previous research has shown that using HNTs as a nanofiller may significantly enhance the compressive strength, compressive modulus, and thermal stability, even when added to polymers at 3–6 wt.% (Liu *et al*. 2013, Naumenko *et al*. 2016).

Polypropylene is one of the most widely used basic polymers in the world. It is made up of the polymerization of propylene under relatively mild temperature and pressure conditions in the presence of catalyst (Busico and Cipullo 2001, Maddah 2016, Shubhra *et al*. 2013). Polypropylene has a variety of properties that have led to its widespread use, particularly in the plastic and fiber industries. One of the most important characteristics of this material compared with polymers, such as polyamides, is their non-absorption of moisture, which has made it a suitable option for many applications. The properties of this material can be improved by making some subsequent modification.

Despite the significant advantages of natural composites, they suffer from various drawbacks, including relatively poor mechanical properties, high flammability, and high moisture absorption. Therefore, materials such as ammonium polyphosphate (APP), HNTs, eggshell powder (ESP), and magnesium hydroxide (MH) have been used in NF composites to partially compensate for some or all the aforementioned drawbacks (Balan *et al*. 2020, Kamarian *et al*. 2022). Regarding composite materials reinforced with AFs, Li *et al*. (2017) investigated the effects of co-incorporation of nanoclay (NC), APP, and HNTs on the flammability, thermal stability, and mechanical properties of abaca-fabric/vinyl ester composites. They showed an increase in the fire resistance of the composite system at the optimal additive content, whereas the tensile and bending parameters exhibited a slight decrease. Nguyen Tran *et al*. (2021) analyzed the effects of biowaste ESP materials on the flammability and mechanical properties of AF/PP composites. They employed the injection molding technique to prepare composite specimens and conducted different experimental tests, including tensile, bending, and horizontal burning tests. The results of this research demonstrated the ability of ESP to decrease the flammability of the structure, while causing a destructive effect on the mechanical properties of the composite system. Shah *et al*. (2013) examined the influence of NC on the flammability and tensile properties of AF/PP composites. At the optimal NC content, they recorded a substantial enhancement in both the tensile properties and the fire resistance of the composite.

During the last decade, the indentation test has become the most popular, standard, and straightforward technique for characterizing various mechanical properties, such as residual stress (Chen *et al*. 2006), elastic modulus (Bao *et al*. 2004, Lee *et al*. 2007), hardness (Mahmoudi and Nourbakhsh 2011, Saber-Samandari and Gross 2009b), stiffness (Molazemhosseini *et al*. 2013, Saber-Samandari and A Gross 2009a) and plasticity index (Barbaz-Isfahani *et al*. 2022). Oliver and Pharr (1992) developed an indentation method for evaluating the mechanical properties of various materials using different indenter shapes. In the indentation test, a controlled load is applied and lifted on a specimen using a geometrically well-defined probe to determine the force-displacement diagram (Gross and Saber-Samandari 2009, Oliver and Pharr 2004) and calculate the mechanical properties of various materials (Saber-Samandari *et al*. 2011, Saber-Samandari and Gross 2009c). For example, Sfarra *et al*. (2013) investigated the mechanical properties of eco-friendly composite laminates using the indentation method. They manufactured a hybrid laminate, including jute Hessian cloth (plain weave) and hemp fibers in an epoxy matrix. The elastic modulus and hardness of the fabricated composite materials were obtained via indentation tests and compared using different non-destructive techniques. Das *et al*. (2009) employed the indentation method to investigate the mechanical performance of graphene-incorporated polyvinyl alcohol and poly(methyl methacrylate) matrix composites. Their results showed a significant increase in the elastic modulus and hardness of the composite specimens only containing 0.6 wt.% of graphene compared with pure composites. Additionally, their study indicated the importance and efficiency of the indentation method in characterizing the mechanical behavior of composite materials. Hosseinzadeh and Mahmoudi (2017) adopted the indentation method with the Knoop and Vickers indenters to measure the mechanical properties based on the force-displacement diagram. They developed a new localized procedure to derive the yield stress, work-hardening exponent, and elastic modulus of the specimens. Shokrieh *et al*. (2013) explored the elastic modulus, hardness, and plasticity index of composite and nanocomposite materials using the indentation method with a Berkovich indenter. Their results indicated an increase in the normal hardness and elastic modulus of the composite specimens with the addition of more nanoparticles to the polymer matrix. Furthermore, the plasticity index of the nanocomposites decreased with the incorporation of nanofillers, indicating an improvement in the elastic recovery of the fabricated specimens.

In addition to experimental approaches, artificial neural networks (ANNs) have been implemented to predict the mechanical properties of materials over a wide range of applications (Guo *et al*. 2021, Ming *et al*. 2021, Wang and Zhang 2021), based on experimental tests' outputs or computerized simulations' results (Cao *et al*. 2006, Haj-Ali

Table 1 Taguchi design of experiments for the composite samples at three levels of 0%, 3% and 6% HNTs, and three levels of 0%, 3% and 6% ESP

No.	Sample Code	Composition	
		HNT (wt.%)	ESP (wt.%)
1	H0E0	0	0
2	H0E3	0	3
3	H0E6	0	6
4	H3E0	3	0
5	H3E3	3	3
6	H3E6	3	6
7	H6E0	6	0
8	H6E3	6	3
9	H6E6	6	6

et al. 2008, Khalvandi *et al*. 2022). In most cases, feed-forward neural networks are employed, in which the input data and the initial conditions considered for designing the experiments are related to laboratory results, which are categorized as the outputs of the neural networks. Relating the data to one another can be considered a linear regression problem. Similar studies that focused on the combination of ANNs and indentation tests suggest the possibility of highly accurate estimation of mechanical properties by extracting force-depth diagrams and calculating the desired properties (Arbabi *et al*. 2016). More specifically, feed-forward ANNs have shown high potential in interpreting and forecasting Vickers hardness with acceptable precision (El-Rehim *et al*. 2020). The efficiency of ANNs in predicting the elastic-plastic properties of composite materials can be proven via indentation tests. For instance, this approach has been employed to estimate the fatigue lifespan (Lee *et al*. 1999, Vassilopoulos *et al*. 2007), detect thermal damage (Sarhadi *et al*. 2022), and investigate the fiber size effects (Uddin *et al*. 2022) in composite materials. Therefore, the application of ANNs can be a suitable choice for constitutive modeling during the material design process.

Regarding the limited research works in the field of AF/PP composites' behavior under indentation test, this study aimed to assess the effects of HNT and ESP additives on the obtained mechanical properties of AF/PP composites via the indentation method. Indentation tests were conducted on the composites with different additives with varying load amplitude using two types of indenters (Vickers or conical). A feed-forward ANN was then trained to predict the mechanical properties of the AF/PP/ESP/HNT composites. The trained network exhibited high accuracy in estimating various parameters, including the Young's modulus, hardness, and plasticity index.

2. Materials and methods

2.1 Preparation of eco-friendly AF/PP/ESP/HNT composite materials

Here the process of preparing AF/PP composite samples with HNT and ESP additives are explained. It should be noted that the basic composite (AF/PP) is composed of 30wt.% AF and 70wt.% PP. In the first step, AFs were cut into fibers with short length. The fibers were then mixed with PP, and the resulting mixture was placed in an oven at 60 ºC overnight and dried. In the next step, the AFs, PP (Chemko S.C.Corp., South Korea), HNT, and ESP (Edentown F&B, Poonglim Industrial Co. Ltd, South Korea.) were poured into an extruder (SJZS-10B, Wuhan Ruiming Experimental Instrument Manufacturing Co., Ltd., China). In the extruder, the mixture passed a path with four different zones at temperatures of 175, 180, 185, and 190 ºC. After leaving the extruder, the molten composite passed over a conveyor in the form of filament that was exposed to a cooling system. The filament was then cooled to room temperature and inserted into a miniature granulator to be turned into pellets of the same size. The process in the extruder and turning into uniform pellets was repeated once more to achieve a more homogeneous composite. The AF/PP/ESP/HNT composite pellets were placed in a mold and subjected to a hot press at 180 ℃ and pressure of 7 MPa. The composite sheet was then released and allowed to cool to room temperature. It was finally cut to dimensions suitable for the indentation test. The manufacturing process of AF/PP/ESP/HNT composites is briefly shown in Fig. 1. Nine different composite sheets were fabricated for three HNT loadings (0, 3 and 6wt.%) and three ESP loadings (0, 3 and 6wt.%), based on Taguchi method (see Table 1).

2.2 Indentation method

The mechanical properties of the fabricated specimens were investigated using an indentation instrument, as shown in Fig. 2. Vickers or conical diamond indenters (Figs. 2b and 2c) were employed to perform normal loads up to 150, 200, and 250 N for each specimen, and the maximum load was maintained for 5 s to reduce the creep effect. The samples were perpendicular to the tip of the indenter during the indentation tests (Saber-Samandari and Gross 2009a). Afterward, the indenter was withdrawn from the specimens at the same rate in the unloading segment. The applied force on the indenter was measured by the load cell, while the penetration depth of the indenter was assessed using a linear movement sensor, as depicted in Fig. 2.

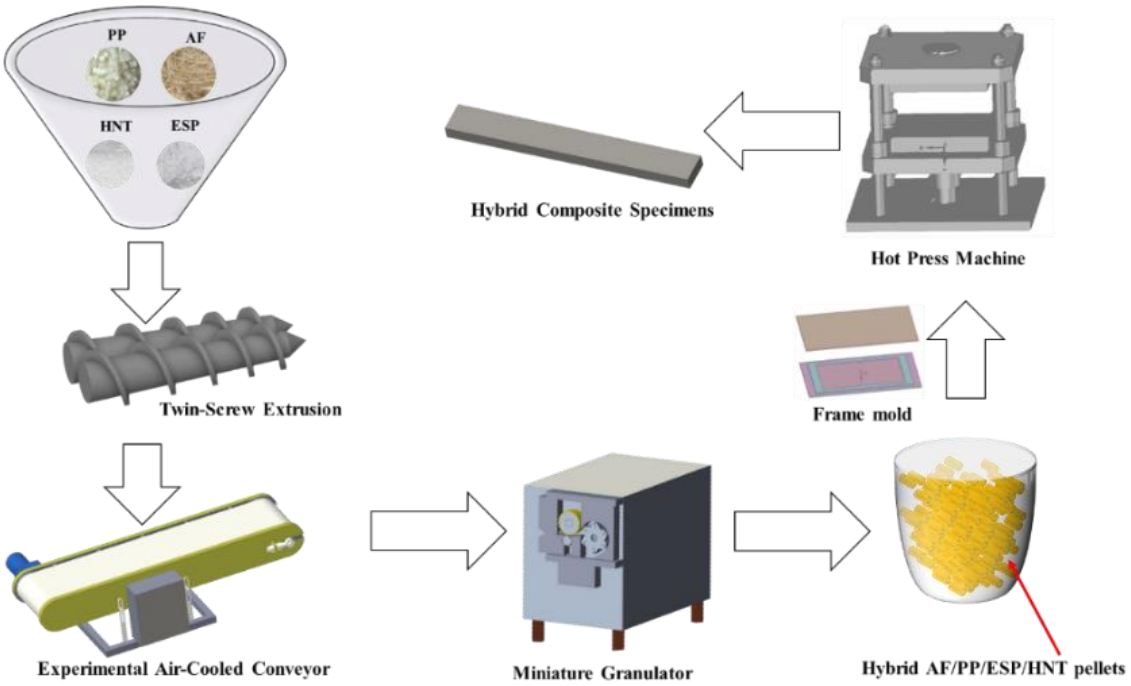

Fig. 1 Schematic of manufacturing process of AF/PP/ESP/HNT composites

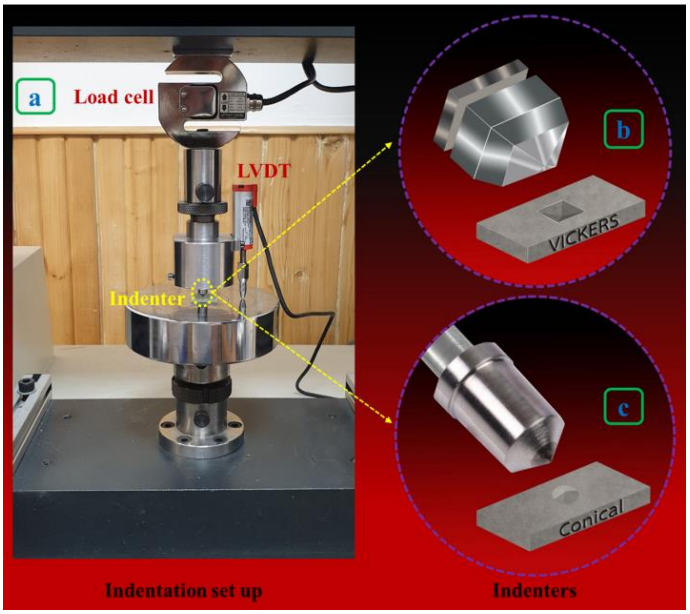

Fig. 2 a) Indentation test setup, and corresponding b) Vickers and c) conical indenters

The loading-unloading diagram of the indentation test is presented in Fig. 3a. According to this diagram, P_{max}, h_{max}, h_c, h_f, and $S = dp/dh$ represent the maximum load, maximum depth, contact depth, final depth, and contact stiffness, respectively. These parameters can be obtained from the load-displacement diagram to calculate the mechanical properties of the specimens. According to the Oliver-Pharr method (Oliver and Pharr 1992), hardness can be calculated using:

$$H = \frac{P_{max}}{A} \tag{1}$$

where Adenotes the projected contact area. According to Figs. 3(b)-(d), the projected contact area of the Vickers and conical plates can be determined by Eqs. (2) and (3) based on Oliver-Pharr reports (Oliver and Pharr 2004, Pharr *et al.* 2009).

$$A = 4{h_c}^2 \tan^2\theta \;\&\theta(Vickers) = 136^\circ \tag{2}$$

$$A = \pi{h_c}^2 \tan^2\psi \;\&\psi(Conical) = 140.6^\circ \tag{3}$$

Moreover, the elastic modulus of specimens can be calculated using:

$$E_r = \frac{\sqrt{\pi}}{2}\frac{dp}{dh}\frac{1}{\sqrt{A}} \tag{4}$$

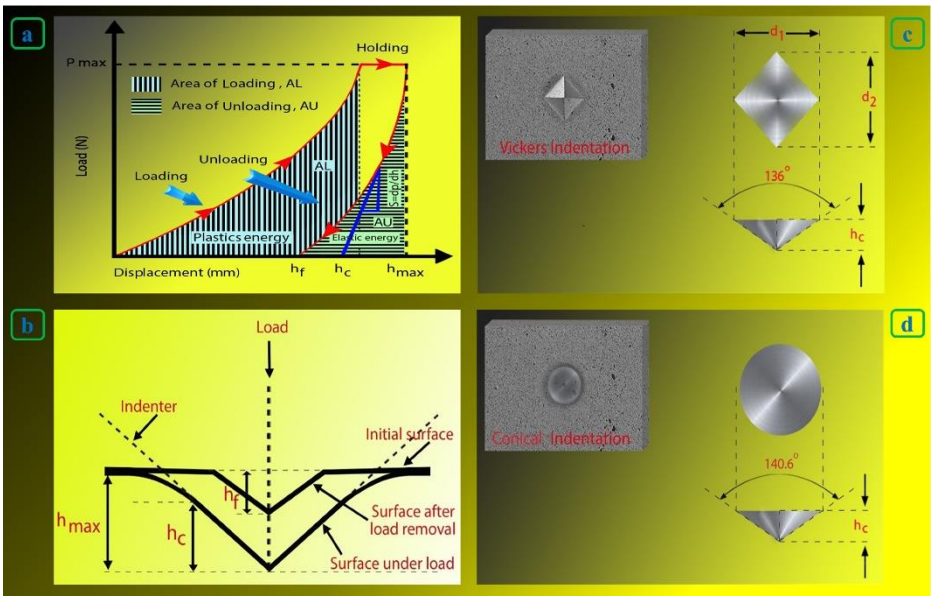

Fig. 3 a) Load-displacement curve in the indentation tests, and schematics of b) contact geometry of indenter and specimens for c) Vickers and d) conical indenters

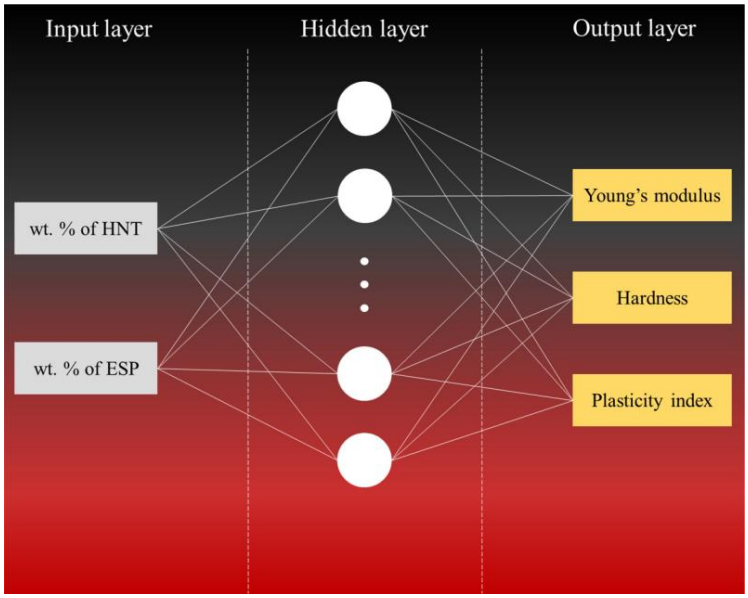

Fig. 4 General schematic representation of the trained ANN

$$\frac{1}{E_r} = \frac{1-{\nu_s}^2}{E_s} + \frac{1-{\nu_i}^2}{E_i} \quad (5)$$

where E_r is the residual modulus of the indentation contact, which can be derived from the load-displacement diagram. E_s and E_i denote the elastic moduli of the specimen and diamond Vickers or conical indenters, respectively ($E_i = 1141GP$) (Gross *et al*. 2010). Moreover, υ_s and υ_i are the Poisson's ratios of the fabricated specimens (equal to 0.35 (Vilaseca *et al*. 2010)) and indenters (equal to 0.07 (Gross *et al*. 2010)), respectively. The plasticity index (ψ) is defined as the elastic-plastic behavior of materials under external forces. The plasticity index can be calculated using the following equation, as reported by (Barbaz-Isfahani *et al*. 2022, Briscoe *et al*. 1998):

$$\psi = \frac{A_l - A_u}{A_l} \quad (6)$$

where A_l and A_u are the areas under the loading and unloading curves (Fig. 3a). The plasticity index ranges from 0 to 1 for polymeric materials with viscoelastic-plastic behavior, $\psi = 0$ indicates fully elastic behavior and $\psi = 1$ represents fully plastic materials.

3. Artificial neural networks

The indentation experiments were conducted on the fabricated composite materials utilizing two types of indenters (Vickers and conical) under various maximum loads of 150, 200, and 250 N. Because the Young's modulus,

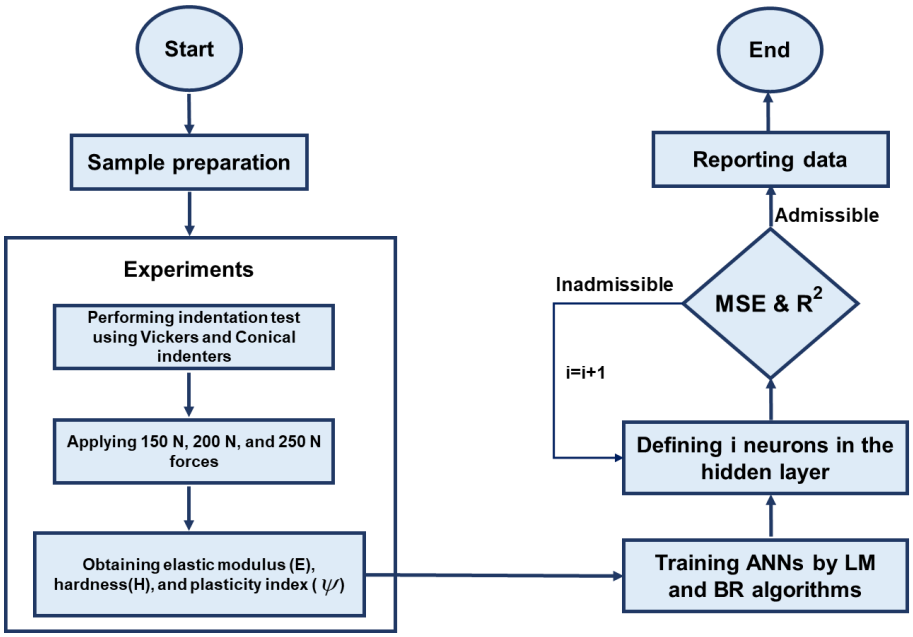

Fig. 5 Flowchart of the research procedure

hardness, and plasticity index are known as the intrinsic properties of the materials, the magnitude of the maximum applied load and indenter type may not result in various values for such material properties. Therefore, only the various weight ratios of HNTs and ESP could affect the Young's modulus, hardness, and plasticity index values. This statement has been graphically presented in subsection 4.3., where no significant difference can be observed among the calculated mechanical properties.

Consequently, a code in MATLAB was developed, and a series of shallow ANNs were trained to predict the Young's modulus, hardness, and plasticity index values of the fabricated composite materials based on the input parameters of the trained networks (i.e., weight ratios of HNTs and ESP). This type of ANN is a feed-forward ANN constituting one input layer with two inputs, one hidden layer containing several neurons, and one output layer with three output data. Our trained ANN functioned based on the backpropagation algorithm, and all the input and output data were normalized by dividing each dataset by the corresponding maximum value.

A schematic of the ANN was presented in Fig. 4. According to this figure, the input parameters were directly connected to all the neurons in the hidden layer. In the first run of the network, the initial weights and biases were randomly defined and specified for each neuron in the hidden layer. Employing Eq. (7), the summation of the calculation process for each neuron is multiplied by a certain function called the activation function, represented by $k(x)$, where W_i and b_i represent the weights and biases, respectively. In this study, the sigmoid function was considered the activation function (Eq. (8)).

To minimize the prediction errors and examine the effect of the networks' learning rule, the Levenberg-Marquardt (LM) algorithm along with the Bayesian Regularization (BR) algorithm were utilized. Afterward, 70% of the experimental data were used during the training process of the ANNs, and the remaining 30% of the data were considered for the testing and/or validation of the trained neural networks. In the case of networks with the LM learning rule, there were three data categories: training, testing, and validation. In contrast, networks with the BR learning rule only held two datasets: training and testing. The data were randomly distributed over the training, testing, and validation categories. After each cycle of error minimization, if necessary, the weights and biases were updated, and the outputs of the networks were calculated using Eq. (7).

$$Output = k(x)\left[\sum_{i=1}^{n} W_i.\ x + b_i\right] \tag{7}$$

$$k(x) = \frac{1}{1+e^{-x}} \tag{8}$$

To study the effects of the number of neurons in the hidden layer, which might have affected the predictions of the trained networks, the number of 1 up to 7 neurons along with 1 up to 10 neurons were defined in the hidden layer, where the LM and BR algorithms were the learning rules of the ANN, respectively.

To clarify the workflow performed in this study, a flowchart showing the complete scheme of the various methods employed, including sample preparation, indentation experiments, and ANN, was presented in Fig. 5.

4. Results and discussion

4.1 Indentation results

As mentioned in the previous section, indentation tests were conducted to evaluate the mechanical properties of the fabricated specimens. Fifty-four indentation tests were

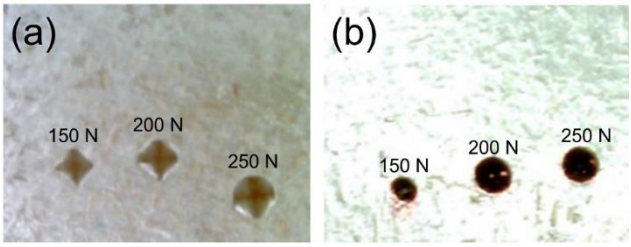

Fig. 6 Residual indentation of a) Vickers and b) conical indenters after applying loads of 150, 200, and 250 N

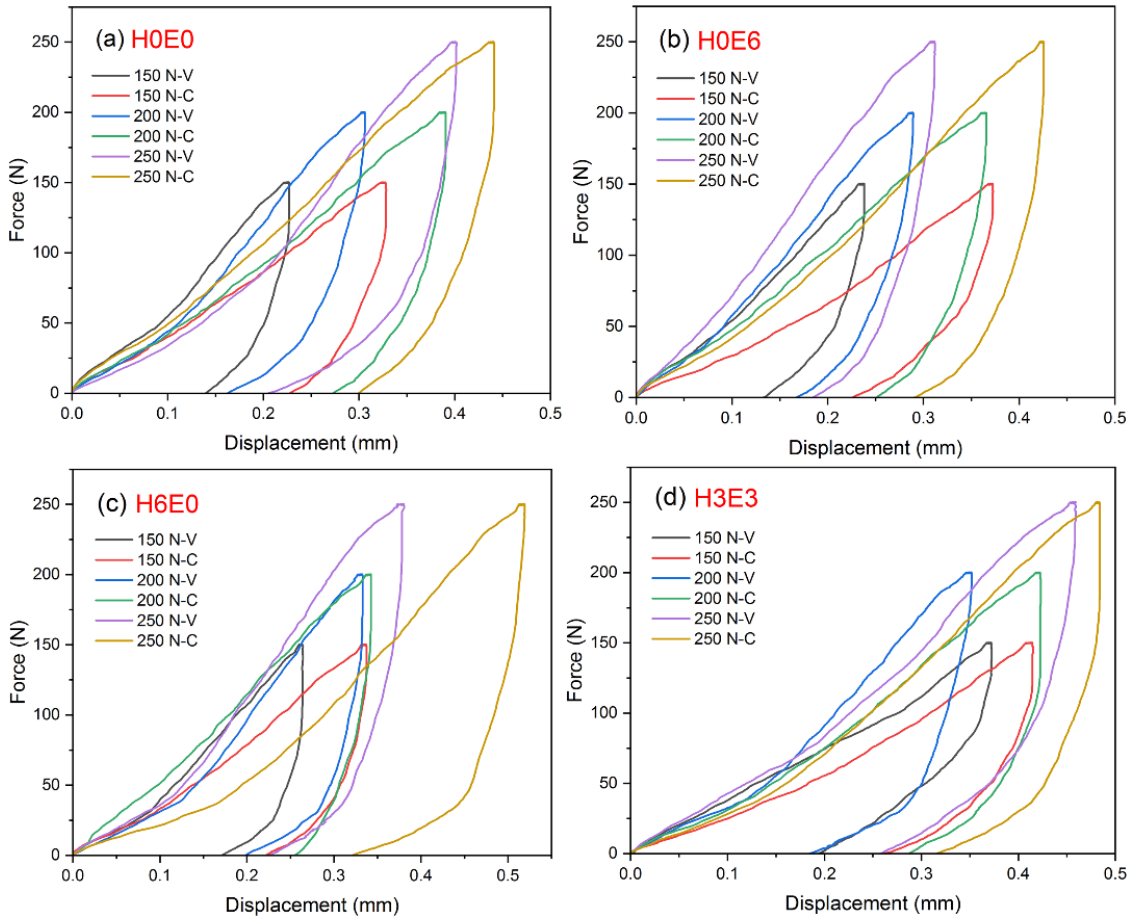

Fig. 7 Indentation load-displacement of specimens with different maximum forces and indenters, including a) H0E0, b) H0E6, c) H6E0, and d) H3E3

performed on nine series of fabricated specimens with various ESP and HNT weight fractions using two indenters (Vickers and conical) under three force amplitudes (150, 200, and 250 N). Based on Fig. 6, the indented spots reveal that the contact area of the indentation increased with enhanced maximum applied force. Fig. 7 displays some of the load-displacement curves obtained from the indentation tests at various maximum loads using different indenters. The naming of the composite systems in Fig. 7 is such that H6E0 represents a composite specimen comprising 6 wt.% HNTs and 3 wt.% ESP, *V* and *C* represent the Vickers and conical indenters, respectively.

As the load-depth results show, the penetration depth of the indenters increased with an increase in the maximum load of the indentation tests. In addition, owing to the sharp shape of the conical indenter, its penetration depth was greater than that of the Vickers indenter in all the specimens. A comparison of the loading and unloading curves of the specimens with different additives indicated that the HNTs were more effective in improving the stiffness of the fabricated specimens than the pure composites. The nanoscale dimensions of HNTs with ideal mechanical properties and high aspect ratios of clay nanoparticles (Gitiara *et al*. 2021, Kamarian *et al*. 2022, Wu *et al*. 2013), compared with the micro-dimensions of ESP, could explain the improvement in the stiffness of the HNT-incorporated composite specimens. The residual elastic modulus and plasticity index of the composite specimens were determined from the force-depth curves. In addition, the elastic modulus and hardness were calculated using Eqs. (1) and (5), respectively. Accordingly, the effects of the HNTs and ESP on the obtained indentation results were discussed further.

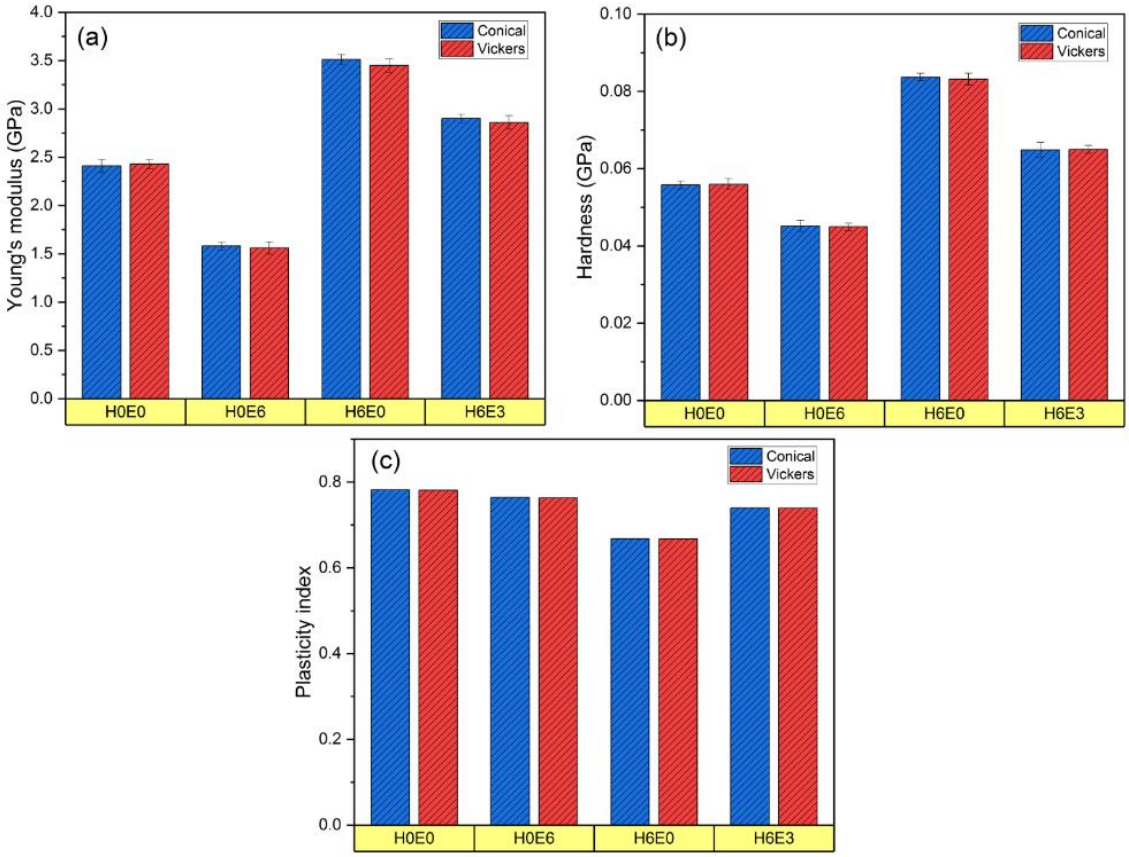

Fig. 8 Comparison between the calculated a) Young's moduli, b) hardness, and c) plasticity indices among the four types of indentation test specimens

4.2 Verification investigation

In this study, the accuracy of the experimental data obtained from the indentation tests was examined. Composite specimens comprising AF and PP, without any additives, were prepared and subjected to indentation tests. Based on the approach described in section 2, the Young's modulus of the specimens was calculated to be 2.36 GPa. Next, tensile specimens made of the same composite (pure AF/PP) were prepared. The ASTM D638 standard was used to conduct tensile tests on the prepared samples. A universal testing machine (R & B Inc., Korea) with a 2.5-t load cell was used to complete the tensile test. The crosshead speed was set at 2 mm/min. From the experimental results, the mean value for the Young's modulus of the composite system was 2.38 GPa, indicating an error of less than 1%. Therefore, it can be concluded that the experimental data from the indentation test were sufficiently accurate to rely on.

4.3 Artificial neural networks

As described in section 3, we normalized the data to be implemented in the prediction process using the trained ANNs by dividing each dataset by its corresponding maximum value. According to the calculated mechanical properties, the maximum Young's modulus and hardness belonged to the H6E0 specimens, while the H0E0 samples exhibited the maximum plasticity index. The indentation test results indicated that the elastic modulus, hardness, and plasticity index were not dependent on the type of indenter and applied maximum force because they were the intrinsic properties of the materials (Fig. 8).

ANNs were employed to investigate the various conditions that might affect the material properties during the indentation tests. Accordingly, various numbers of neurons were defined in the hidden layer to relate the inputs to the outputs. In general, two factors were encountered after the convergence of the trained ANNs' calculations.

The first parameter for interpreting ANN results was themean squared error (MSE). We expected the gradual convergence of this parameter for each dataset and its reduction at each epoch with respect to its corresponding latest epoch. More specifically, the MSE reduced at any subsequent epoch of the ANN. Moreover, a higher number of neurons in the hidden layer may affect the MSE, the higher the number of neurons, the lower the MSE. The MSE is usually defined by Eq. (9), where Y_{Exp} and Y_{Net} represent the experimental data and predictions of the trained ANNs, respectively.

In addition to the MSE, we introduced another index called the determination coefficient, R^2, to monitor the predictions of the networks and their accuracy. This parameter is given by Eq. (10), where $\overline{Y_{Exp}}$ is the mean value of the experimental data. Higher values for this index, reaching the magnitude of 1, indicate the accuracy of the predictions, thus, the trained ANN can properly estimate the behavior of the material based on the input and output data.

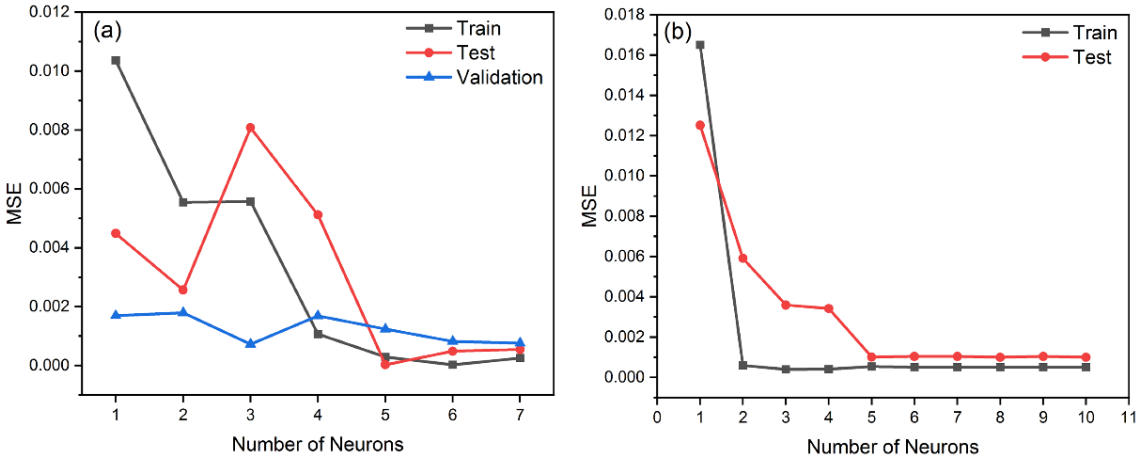

Fig. 9 MSE trends of the train, test, and validation data, with ANN learning rules of a) Levenberg-Marquardt (LM) algorithm and b) Bayesian regularization (BR) algorithm

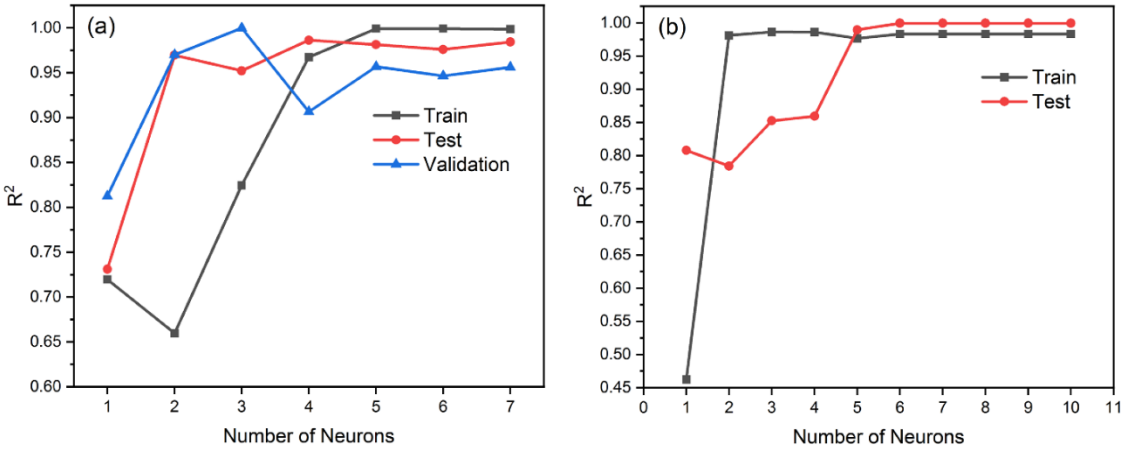

Fig. 10 Variation of R^2, for ANN learning rules of a) LM algorithm and b) BR algorithm

$$MSE = \frac{1}{n}\left[\sum_{i=1}^{n}(Y_{Exp}^{i} - Y_{Net}^{i})^2\right] \quad (9)$$

$$R^2 = 1 - \frac{\sum_{i=1}^{n}(Y_{Exp}^{i} - Y_{Net}^{i})^2}{(Y_{Exp}^{i} - \overline{Y}_{Exp})^2} \quad (10)$$

The ANNs could make desirable predictions of the experimental data, where LM algorithm trained the ANNs and the number of neurons increased to 7. In the case of using the BR algorithm, the best predictions were attained by the network with ten neurons in the hidden layer. To clarify this, we refer to the variations in the MSE value with respect to the number of neurons in the hidden layer.

Fig. 9a presents the MSE values versus the number of neurons in the hidden layer of the ANN, where the LM algorithm is the learning rule of the trained networks. As can be seen, the worst predictions belong to ANNs with 1–4 neurons in their hidden layers, where the MSE values of the training, test, and validation data fluctuate. In contrast, when the number of neurons in the hidden layer varied from 5 to 7, a semi-stable MSE trend was observed. Specifically, as the number of neurons in the hidden layer reached 7, the MSEs were close to each other. Consequently, when LM is the learning rule of the trained ANNs, the best prediction was made by the ANN with a 2×7×3 configuration, in which 2, 7, and 3 represent the number of inputs, neurons in the hidden layer, and output parameters, respectively.

As stated previously, we used two different learning rules for feed-forward ANNs, and we now discuss the trend of the calculated MSE as a function of the neurons in the hidden layer of the ANNs whose governing algorithm is BR. In these ANNs, when we defined 1–5 neurons in the hidden layer, the MSE values, particularly for the test data, decreased or fluctuated. More specifically, no stable trend was observed. When we considered 6–10 neurons in the hidden layer of the trained ANNs, the MSE values of the train and test data remained constant, and no further decrease was observed. Therefore, in the case of ANNs with the BR algorithm as learning rule, the desired network configuration was 2×10×3 (Fig. 9b).

Comparing the LM and BR algorithms, we found that the BR algorithm was more robust than the LM algorithm regarding the MSE because the decreasing trend of the corresponding MSEs was smoother with the least fluctuations.

In contrast to the MSE, which exhibits a decreasing trend with an increasing number of neurons in the hidden layer, R^2 increased as the number of neurons was increased.

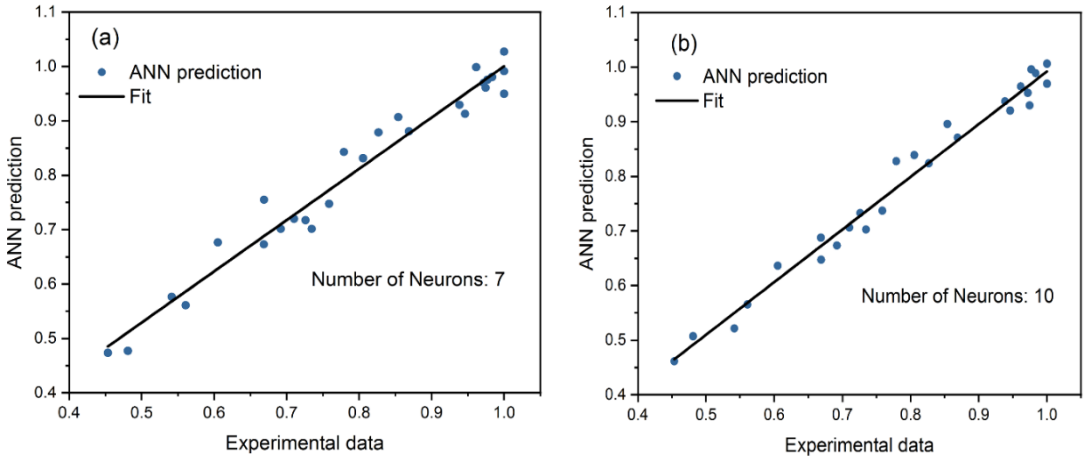

Fig. 11 Applied regression to all data based on the a) LM algorithm and b) BR algorithm

The ideal value of R^2 is 1, thus, as this parameter approaches 1, we can trust the accuracy of the trained ANN. This implies that the predictions of the ANNs are close to the input data. In other words, where $R^2 = 1$, the predictions of the ANNs and experimental data are the same, and if we plot the data with respect to each other, we would realize that the fitting function will be $Y=X$.

Fig. 10a depicts the variations in R^2, where the LM algorithm is the learning rule of the ANNs. Considering 1–4 neurons in the hidden layer, the R^2 value fluctuates between 0.66 and 0.98, indicating that 66% and 98% of the data were around the regression line, respectively. Whereas, when the number of neurons in the hidden layer varied from 5 to 7, 95.6% and 99% of the data were close to linear regression. Consequently, in this case, the proper configuration of the hidden layer contains 7 neurons.

For the second type of trained ANNs with the BR algorithm as the learning rule, R^2 values were in the range of 0.46 up to 0.99, where 1–5 neurons were defined in the hidden layer (Fig. 10b). Afterward, where 6–10 neurons were defined in the hidden layer, the R^2 values stood around 0.98 and 0.99 for the test and train data, respectively. This implies that 98% and 99% of the test and train data lie on the regression line or are located in the neighborhood of this line. Therefore, the BR algorithm performs better than the LM algorithm as a learning rule (Fig. 11).

As a concluding remark on the trained ANNs, the BR algorithm provided more precise predictions than the LM algorithm. Consequently, we considered the network with a 2×10×3 configuration as the desirable network, which was trained by the BR algorithm. This network had two input parameters (i.e., weight ratios of HNTs and ESP), 10 neurons in the hidden layer, and 3 output parameters (i.e., Young's modulus, hardness, and plasticity index). Our interpretation of the fabricated composites under the indentation test was based on the predictions of the trained ANN, which have been depicted in Fig. 12.

4.4 Effects of HNTs and ESP on mechanical properties of AF/PP composites using ANN

As aforementioned, the effect of incorporating HNTs and ESP on the mechanical behavior of filled eco-friendly AF-reinforced composites was predicted using ANNs. Fig. 12 depicts the contour of the Young's modulus behavior with various loadings of HNTs and ESP into the AF/PP composites, indicating the effect of different loadings of HNTs and ESP. The results indicate that the addition of HNTs increased the Young's modulus of the composite specimens. For instance, the Young's moduli of composite specimens containing 3 and 6 wt.% of HNTs increased by 25.7% and 44.4% compared with neat specimens, respectively. As mentioned earlier, the ideal mechanical properties of the HNTs and their high aspect ratios could explain the variations in the mechanical properties of the composite specimens containing HNTs. Relatively similar behavior was observed by previous researchers regarding the effect of NC on the Young's modulus of AF-reinforced composites. Shah *et al.* (2013) showed that as the NC content increased to 15%, the tensile modulus of PP/AF composites increased. Furthermore, Manickam *et al.* (Manickam *et al.* 2021) observed that adding up to 4% NC increased the tensile modulus of glass/abaca hybrid epoxy composites. Based on the results displayed in Fig. 12, it was concluded that, owing to their lower mechanical properties and aspect ratio, adding ESP into the composite specimens could significantly decrease their Young's modulus. For example, the Young's modulus of a composite with 3 wt.% of ESP decreased by 30.7% compared with the pure composite, while increasing the weight fraction of ESP up to 6% decreased the Young's modulus by 34.8%. The ESP agglomeration and the micro-size of ESP particles could increase the stress concentration of composites filled with these particles, which could also cause the reduction in the mechanical properties. In a similar study on PP/AF composites, Nguyen Tran *et al.* (2021) observed that with an increase in the ESP loading (up to 4%), the tensile modulus of the composite samples decreased. The results were obtained for a composite system comprising 15% AF.

Meanwhile, the simultaneous addition of HNTs and ESP increased the Young's modulus of the composite specimens compared with the neat composite specimen. However, the enhancement of the Young's modulus for specimens containing both HNTs and ESP particles was lower than

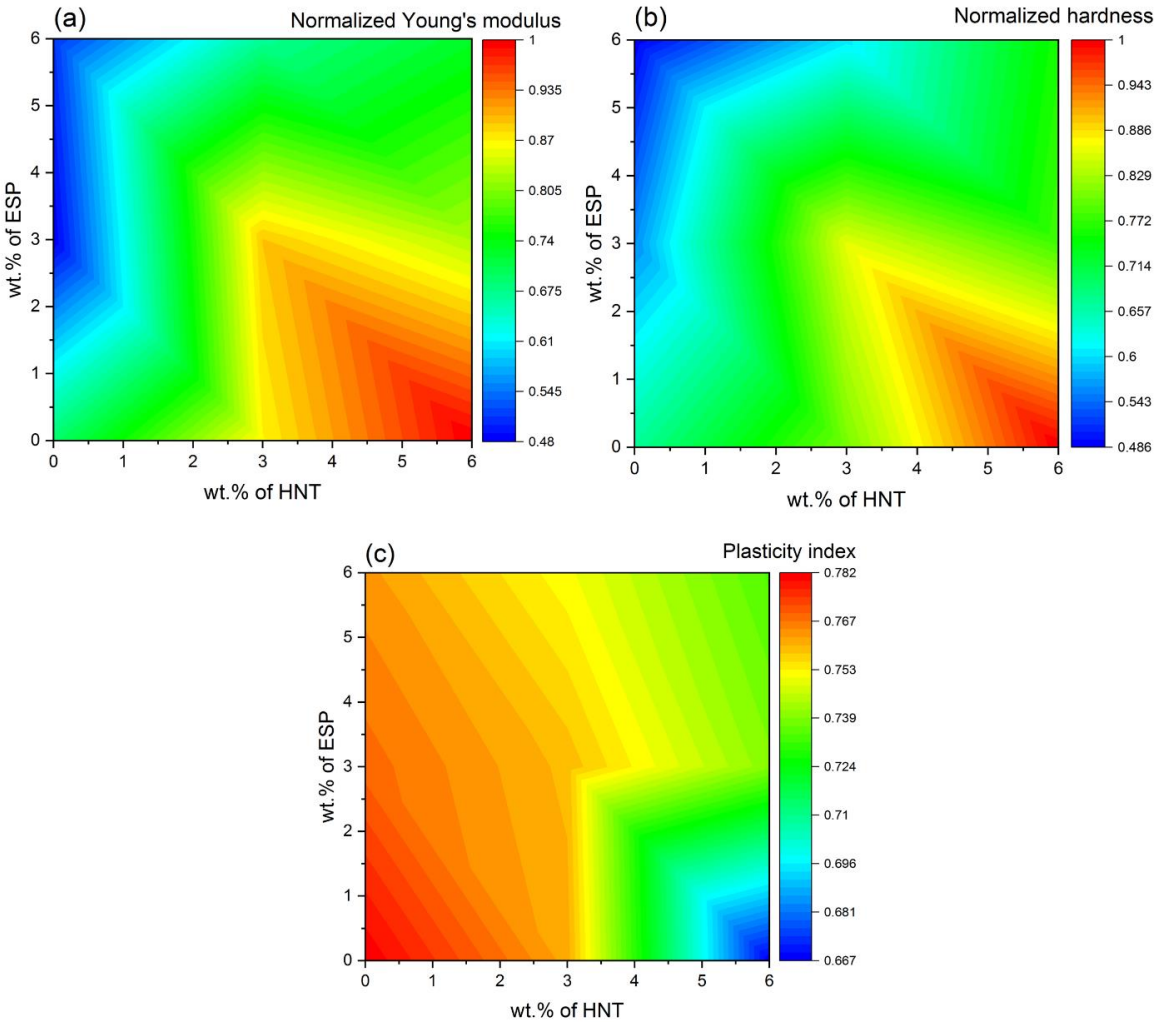

Fig. 12 Distribution contours of a) Young's modulus, b) hardness, and c) plasticity index of incorporated AF/PP composites with different HNT and ESP loadings based on the ANN's predictions

that for specimens incorporating only HNTs. For example, the Young's modulus of the specimen incorporated with 6 wt.% HNTs along with 6 wt.% ESP increased by approximately 4.5%. From comparing the results in Fig. 12a, increasing the addition of ESP in the hybrid-filled composites resulted in reduced mechanical properties, whereas, incorporation of more HNTs could increase the Young's modulus of hybrid composites due to the reason discussed earlier.

Fig. 12b illustrates the contour of the hardness behavior obtained using the ANN method, indicating the effect of various loadings of HNTs and ESP particles in eco-friendly AF-reinforced composites. The same increasing trend was observed for the hardness with the addition of HNTs into the fabricated composites and reduced hardness with incorporation of ESP particles. Moreover, incorporation of both fillers enhanced the hardness, particularly for specimens containing more HNTs. Shokrieh *et al*. (Shokrieh *et al*. 2013) reported that hardness defines the resistance of a material to deformation caused by normal forces. Thus, by incorporating HNTs with high intrinsic strength and aspect ratio into the composite specimens, the indenter interacts with stiffer materials. In addition, the addition of ESP decreased the mechanical properties, leading to a reduction in hardness. The trend of the hardness indicates that incorporation of more ESP decreases the hardness of the composites containing both HNTs and ESP particles. For instance, the calculated hardness of the specimens incorporated with 6 wt.% ESP + 3 wt.% HNTs was approximately 0.0502 GPa, while the hardness of filled composites with 3 wt.% ESP + 6 wt.% HNTs was approximately 0.0649 GPa. The contours of the plasticity index behavior based on various loadings of the HNT and ESP fillers are shown in Fig. 12c. As reported by Barbaz-Isfahani (2022), the plasticity index (Ψ) defines the elastic-plastic behavior of materials under external forces. From the results, the plasticity indices of all the composite specimens were between 0 and 1, indicating their viscoelastic-plastic behavior. Moreover, the addition of HNTs and ESP decreased the plasticity index of the specimens, compared with pure composites, suggesting an increase in the elastic recovery of filler-incorporated composites. Thus, the filled composite specimens tended to behave elastically compared with the neat ones. The addition of nano- and micro-fillers could increase the brittleness of the filled composites, which could lead to a

decrease in their plasticity indices. The reduction in the plasticity index for specimens containing HNTs was more significant than that for the specimens constituting ESP particles. For example, the plasticity index of the specimen containing 6 wt.% of HNTs decreased by 14.6% compared with pure composites, while the plasticity index of composites filled with 6 wt.% of ESP decreased by only 2.3%.

5. Conclusions

In the present work, an indentation test was firstly performed on AF/PP composites incorporated with HNTs and ESP. The experimental datasets were obtained from indentation tests for different HNT and ESP loadings, load amplitudes, and two indenters. An ANN with high accuracy was then trained based on the indentation experimental data to predict the mechanical properties of the composites, including the Young's modulus, hardness, and plasticity index.

• The code developed for generating a shallow ANN, whose learning rule was Bayesian Regularization algorithm and had ten neurons in the hidden layer could act as a robust predictor, with the lowest MSE and the highest accuracy, regarding the ANN predictions and experimental data from indentation test. Furthermore, fitting a linear regression revealed that this trained ANN had the potential of estimating the variation of the mechanical properties based on the intrinsic properties of materials and the laboratory conditions.

• The indentation results showed that the addition of HNTs could increase the elastic modulus and hardness of the fabricated composites, whereas, the incorporation of ESP reduced the mechanical properties. Furthermore, the addition of both HNTs and ESP increased the Young's modulus of the composite specimens compared with the pure AF/PP composite. However, the enhancement of Young's modulus for specimens containing hybrid HNT-ESP particles was lower than that for specimens incorporating only HNTs.

• The hardness of the specimens increased with the addition of HNTs into the fabricated composites, and reduced with the incorporation of ESP. Moreover, the incorporation of both fillers enhanced the hardness, particularly for specimens containing more HNTs.

• The plasticity indices of all the composite specimens ranged between 0 and 1, indicating the viscoelastic-plastic behavior of the fabricated composite specimens. The reduction in the plasticity index for specimens containing HNTs was more significant than that for the specimens comprising ESP particles, indicating that the composite specimens filled with HNTs tended to behave more elastically.

Acknowledgments

This research was supported by Basic Science Research Program through the National Research Foundation of Korea (NRF) funded by the Ministry of Education (No. 2018R1A6A1A03024509).

References

Arbabi, V., Pouran, B., Campoli, G., Weinans, H. and Zadpoor, A.A. (2016), "Determination of the mechanical and physical properties of cartilage by coupling poroelastic-based finite element models of indentation with artificial neural networks", *J. Biomech*., **49**(5), 631-637. https://doi.org/10.1016/j.jbiomech.2015.12.014.

Balan, G.S., Krishnan, A.M., Saravanavel, S. and Ravichandran, M. (2020), "Investigation of hardness characteristics of waste plastics and egg shell powder reinforced polymer composite by stirring route", *Mater. Today*, **33**(4090-4093). https://doi.org/10.1016/j.matpr.2020.06.545.

Bao, Y., Wang, W. and Zhou, Y. (2004), "Investigation of the relationship between elastic modulus and hardness based on depth-sensing indentation measurements", *Acta Mater*., **52**(18), 5397-5404. https://doi.org/10.1016/j.actamat.2004.08.002.

Barba, B.J.D., Madrid, J.F. and Penaloza Jr, D.P. (2020), "A review of abaca fiber-reinforced polymer composites: Different modes of preparation and their applications", *J. Chilean Chem. Soc*., **65**(3), 4919-4924. http://doi.org/10.4067/s0717-97072020000204919

Barbaz-Isfahani, R., Saber-Samandari, S. and Salehi, M. (2022), "Novel electrosprayed enhanced microcapsules with different nanoparticles containing healing agents in a single multicore microcapsule", *Int. J. Biol. Macromol*., **200**, 532-542. https://doi.org/10.1016/j.ijbiomac.2022.01.084.

Briscoe, B., Fiori, L. and Pelillo, E. (1998), "Nano-indentation of polymeric surfaces", *J. Phys. D*., **31**(19), 2395. http://doi.org/10.1088/0022-3727/31/19/006.

Busico, V. and Cipullo, R. (2001), "Microstructure of polypropylene", *Prog. Polym. Sci*., **26**(3), 443-533. https://doi.org/10.1177/0892705711428659.

Cao, L., Youn, I., Guilak, F. and Setton, L.A. (2006), "Compressive properties of mouse articular cartilage determined in a novel micro-indentation test method and biphasic finite element model", *J. Biomech. Eng*., **128**(5), 766-771. https://doi.org/10.1115/1.2246237.

Chen, X., Yan, J. and Karlsson, A.M. (2006), "On the determination of residual stress and mechanical properties by indentation", *Mater. Sci. Eng. A*, **416**(1-2), 139-149. https://doi.org/10.1016/j.msea.2005.10.034.

Das, B., Prasad, K.E., Ramamurty, U. and Rao, C. (2009), "Nano-indentation studies on polymer matrix composites reinforced by few-layer graphene", *Nanotechnology*, **20**(12), 125705. https://doi.org/10.1088/0957-4484/20/12/125705.

Deng, S., Zhang, J., Ye, L. and Wu, J. (2008), "Toughening epoxies with halloysite nanotubes", *Polymer*, **49**(23), 5119-5127. https://doi.org/10.1016/j.polymer.2008.09.027.

El-Rehim, A., Alaa, F., Zahran, H.Y., Habashy, D.M. and Al-Masoud, H.M. (2020), "Simulation and prediction of the vickers hardness of AZ91 magnesium alloy using artificial neural network model", *Crystals*, **10**(4), 290. https://doi.org/10.3390/cryst10040290.

Gitiara, Y., Barbaz-Isfahani, R., Saber-Samandari, S. and Sadighi, M. (2021), "Low-velocity impact behavior of incorporated GFRP composites with nanoclay and nanosilica in a corrosive environment: Experimental and numerical study", *J. Compos. Mater*., **55**(27), 3989-4010. https://doi.org/10.1177%2F00219983211031644.

Gross, K.A. and Saber-Samandari, S. (2009), "Revealing mechanical properties of a suspension plasma sprayed coating with nanoindentation", *Surface Coatings Technol*., **203**(20-21), 2995-2999. https://doi.org/10.1016/j.surfcoat.2009.03.007.

Gross, K.A., Saber-Samandari, S. and Heemann, K.S. (2010), "Evaluation of commercial implants with nanoindentation defines future development needs for hydroxyapatite coatings",

J. Biomed. Mater. Res. B., **93**(1), 1-8. https://doi.org/10.1002/jbm.b.31537.

Guo, X., Liu, Y. and Wang, G. (2021), "Computer modeling for frequency performance of viscoelastic magneto-electro-elastic annular micro/nanosystem via adaptive tuned deep learning neural network optimization", *Adv. Nano Res.*, **11**(2), 203-218. https://doi.org/10.12989/anr.2021.11.2.203.

Haj-Ali, R., Kim, H.K., Koh, S.W., Saxena, A. and Tummala, R. (2008), "Nonlinear constitutive models from nanoindentation tests using artificial neural networks", *Int. J. Plast.*, **24**(3), 371-396. https://doi.org/10.1016/j.ijplas.2007.02.001.

Hosseinzadeh, A. and Mahmoudi, A. (2017), "Determination of mechanical properties using sharp macro-indentation method and genetic algorithm", *Mech. Mater.*, **114**(57-68). https://doi.org/10.1016/j.ijplas.2007.02.001.

Jena, D.K. and Sahoo, P.K. (2019), "New strategies for the construction of eggshell powder reinforced starch based fire hazard suppression biomaterials with tailorable thermal, mechanical and oxygen barrier properties", *Int. J. Biol. Macromol.*, **140**(496-504). https://doi.org/10.1016/j.ijbiomac.2019.08.156.

Jirimali, H.D., Chaudhari, B.C., Khanderay, J.C., Joshi, S.A., Singh, V., Patil, A.M. and Gite, V.V. (2018), "Waste eggshell-derived calcium oxide and nanohydroxyapatite biomaterials for the preparation of LLDPE polymer nanocomposite and their thermomechanical study", *Polym. Plast. Technol. Eng.*, **57**(8), 804-811. https://doi.org/10.1080/03602559.2017.1354221.

Kamarian, S. and Song, J.I. (2022), "Review of literature on eco-friendly sandwich structures made of non-wood cellulose fibers", *J. Sandwich Struct. Mater.*, **24**(3), 1653-1705. https://doi.org/10.1177%2F10996362211062372.

Kamarian, S., Yu, R. and Song, J.I. (2022), "Synergistic effects of halloysite nanotubes with metal and phosphorus additives on the optimal design of eco-friendly sandwich panels with maximum flame resistance and minimum weight", *Nanotechnol. Rev.*, **11**(1), 252-265. https://doi.org/10.1515/ntrev-2022-0014.

Kang, D.J., Pal, K., Park, S.J., Bang, D.S. and Kim, J.K. (2010), "Effect of eggshell and silk fibroin on styrene–ethylene/butylene–styrene as bio-filler", *Mater. Des.*, **31**(4), 2216-2219. https://doi.org/10.1016/j.matdes.2009.10.033.

Khalvandi, A., Mohammadi Aghdam, M. and Saber-Samandari, S. (2022), "Fabrication, experimental study, and 2-D finite element computational homogenization of bone scaffolds under uniaxial and biaxial compressive loadings", *Proceedings of the Institution of Mechanical Engineers, Part N: Journal of Nanomaterials, Nanoengineering and Nanosystems*, **236**(3-4), 117-128. https://doi.org/10.1177/23977914221082900.

Khalvandi, A., Saber-Samandari, S. and Aghdam, M.M. (2022), "Application of artificial neural networks to predict Young's moduli of cartilage scaffolds: An in-vitro and micromechanical study", *Biomater. Adv.*, 212768. https://doi.org/10.1016/j.bioadv.2022.212768.

Lee, H., Mall, S., He, P., Shi, D., Narasimhadevara, S., Yun, Y.H., Shanov, V. and Schulz, M.J. (2007), "Characterization of carbon nanotube/nanofiber-reinforced polymer composites using an instrumented indentation technique", *Compos. Part B Eng.*, **38**(1), 58-65. https://doi.org/10.1016/j.compositesb.2006.04.002.

Lee, J., Almond, D. and Harris (1999), "The use of neural networks for the prediction of fatigue lives of composite materials", *Compos. Part A Appl. Sci. Manuf.*, **30**(10), 1159-1169. https://doi.org/10.1016/S1359-835X(99)00027-5.

Li, Z., Shah, A.R., Prabhakar, M. and Song, J.-i. (2017), "Effect of inorganic fillers and ammonium polyphosphate on the flammability, thermal stability, and mechanical properties of abaca-fabric/vinyl ester composites", *Fibers Polym.*, **18**(3), 555-562. https://doi.org/10.1007/s12221-017-6859-7.

Liu, K., Takagi, H. and Yang, Z. (2013), "Dependence of tensile properties of abaca fiber fragments and its unidirectional composites on the fragment height in the fiber stem", *Compos. Part A Appl. Sci. Manuf.*, **45**(14-22). https://doi.org/10.1016/j.compositesa.2012.09.006.

Liu, M., Guo, B., Zou, Q., Du, M. and Jia, D. (2008), "Interactions between halloysite nanotubes and 2, 5-bis (2-benzoxazolyl) thiophene and their effects on reinforcement of polypropylene/halloysite nanocomposites", *Nanotechnology*, **19**(20), 205709. https://doi.org/10.1088/0957-4484/19/20/205709.

Liu, M., Wu, C., Jiao, Y., Xiong, S. and Zhou, C. (2013), "Chitosan–halloysite nanotubes nanocomposite scaffolds for tissue engineering", *J. Mater. Chem. B*, **1**(15), 2078-2089. https://doi.org/10.1039/C3TB20084A.

Maddah, H.A. (2016), "Polypropylene as a promising plastic: A review", *Am. J. Polym. Sci*, **6**(1), 1-11. https://doi.org/10.5923/j.ajps.20160601.01.

Madsen, B. and Gamstedt, E.K. (2013), "Wood versus plant fibers: Similarities and differences in composite applications", *Adv. Mater. Sci. Eng.*, 2013. https://doi.org/10.1155/2013/564346.

Mahmoudi, A. and Nourbakhsh, S. (2011), "A neural networks approach to characterize material properties using the spherical indentation test", *Procedia Eng.*, **10**(3062-3067). https://doi.org/10.1520/JTE20130236.

Mai Nguyen Tran, T., Mn, P., Lee, D.W., Cabo, M., Jr and Song, J.I. (2021), "Polypropylene/abaca fiber eco-composites: Influence of bio-waste additive on flame retardancy and mechanical properties", *Polym. Compos.*, **42**(3), 1356-1370. https://doi.org/10.1002/pc.25906.

Manickam, S., Kannan, T.K., Simon, B.L., Rathanasamy, R. and Raj, S.S. (2021), "Influence of Nanoclay on the technical properties of Glass-Abaca hybrid Epoxy composite", *Polímeros*, **30**. https://doi.org/10.1590/0104-1428.08520.

Manickavasagam, V.M., Vijaya Ramnath, B., Elanchezhian, C., Vignesh, V., Vijai Rahul, V., Sathya Narayanan, S.U. and Tamilselvan, V. (2014), "Investigation on compression and hardness properties of abaca and manila hybrid composite", *Appl. Mech. Mater.*, **680**, 23-26. https://doi.org/10.4028/www.scientific.net/AMM.680.23.

Massaro, M., Lazzara, G., Milioto, S., Noto, R. and Riela, S. (2017), "Covalently modified halloysite clay nanotubes: synthesis, properties, biological and medical applications", *J. Mater. Chem. B*, **5**(16), 2867-2882. https://doi.org/10.1039/C7TB00316A.

Ming, Y., Zandi, Y., Gholizadeh, M., Oslub, K., Khadimallah, M.A. and Issakhov, A. (2021), "Computer simulation for stability performance of sandwich annular system via adaptive tuned deep learning neural network optimization", *Adv. Nano Res.*, **11**(1), 83-99. https://doi.org/10.12989/anr.2021.11.1.083.

Molazemhosseini, A., Tourani, H., Naimi-Jamal, M. and Khavandi, A. (2013), "Nanoindentation and nanoscratching responses of PEEK based hybrid composites reinforced with short carbon fibers and nano-silica", *Polym. Test.*, **32**(3), 525-534. https://doi.org/10.1016/j.polymertesting.2013.02.001.

Naumenko, E.A., Guryanov, I.D., Yendluri, R., Lvov, Y.M. and Fakhrullin, R.F. (2016), "Clay nanotube–biopolymer composite scaffolds for tissue engineering", *Nanoscale*, **8**(13), 7257-7271. https://doi.org/10.1039/C6NR00641H.

Ochi, S. (2006), "Development of high strength biodegradable composites using Manila hemp fiber and starch-based biodegradable resin", *Compos. Part A Appl. Sci. Manuf.*, **37**(11), 1879-1883. https://doi.org/10.1016/j.compositesa.2005.12.019.

Oliver, W.C. and Pharr, G.M. (1992), "An improved technique for determining hardness and elastic modulus using load and displacement sensing indentation experiments", *J. Mater. Res.*, **7**(6), 1564-1583. https://doi.org/10.1557/JMR.1992.1564.

Oliver, W.C. and Pharr, G.M. (2004), "Measurement of hardness

and elastic modulus by instrumented indentation: Advances in understanding and refinements to methodology", *J. Mater. Res.*, **19**(1), 3-20. https://doi.org/10.1557/jmr.2004.19.1.3.

Pharr, G.M., Strader, J.H. and Oliver, W. (2009), "Critical issues in making small-depth mechanical property measurements by nanoindentation with continuous stiffness measurement", *J. Mater. Res.*, **24**(3), 653-666. https://doi.org/10.1557/jmr.2009.0096.

Saber-Samandari, S., Berndt, C.C. and Gross, K.A. (2011), "Selection of the implant and coating materials for optimized performance by means of nanoindentation", *Acta biomaterialia*, **7**(2), 874-881. https://doi.org/10.1016/j.actbio.2010.09.023.

Saber-Samandari, S. and Gross, K.A. (2009a), "Effect of angled indentation on mechanical properties", *J. Eur. Ceram. Soc.*, **29**(12), 2461-2467. https://doi.org/10.1016/j.jeurceramsoc.2009.03.010.

Saber-Samandari, S. and Gross, K.A. (2009b), "Micromechanical properties of single crystal hydroxyapatite by nanoindentation", *Acta Biomaterialia*, **5**(6), 2206-2212. https://doi.org/10.1016/j.actbio.2009.02.009.

Saber-Samandari, S. and Gross, K.A. (2009c), "Nanoindentation reveals mechanical properties within thermally sprayed hydroxyapatite coatings", *Surface Coat. Technol.*, **203**(12), 1660-1664. https://doi.org/10.1016/j.surfcoat.2008.12.025.

Santos, A.C., Ferreira, C., Veiga, F., Ribeiro, A.J., Panchal, A., Lvov, Y. and Agarwal, A. (2018), "Halloysite clay nanotubes for life sciences applications: From drug encapsulation to bioscaffold", *Adv. Colloid Interf. Sci.*, **257**(58-70). https://doi.org/10.1016/j.cis.2018.05.007.

Sarhadi, A., Albuquerque, R.Q., Demleitner, M., Ruckdäschel, H. and Eder, M.A. (2022), "Machine learning based thermal imaging damage detection in glass-epoxy composite materials", *Compos. Struct.*, 115786. https://doi.org/10.1016/j.compstruct.2022.115786.

Sfarra, S., Ibarra-Castanedo, C., Santulli, C., Sarasini, F., Ambrosini, D., Paoletti, D. and Maldague, X. (2013), "Eco-Friendly laminates: From the indentation to non- destructive evaluation by optical and infrared monitoring techniques", *Strain*, **49**(2), 175-189. https://doi.org/10.1111/str.12026.

Shah, A.R., Lee, D.W., Kim, S., Kim, B.S. and Song, J.I. (2013), "Tensile and fire retardant properties of nanoclay reinforced Abaca/Polypropylene composite", *Proceedings of the 2013 International Conference on Aerospace Science & Engineering (ICASE)*, IEEE, 1-5., August. https://doi.org/10.1109/ICASE.2013.6785562.

Shaik, M.S. and Subramanian, H.S. (2021), "An experimental investigation on low-velocity impact response of abaca/epoxy bio-composite", *J. Natural Fiber.*, 1-16. https://doi.org/10.1080/15440478.2021.1941485.

Shokrieh, M., Hosseinkhani, M., Naimi-Jamal, M. and Tourani, H. (2013), "Nanoindentation and nanoscratch investigations on graphene-based nanocomposites", *Polym. Test.*, **32**(1), 45-51. https://doi.org/10.1016/j.polymertesting.2012.09.001.

Shubhra, Q.T., Alam, A.M. and Quaiyyum, M.A. (2013), "Mechanical properties of polypropylene composites: A review", *J. Thermoplast. Compos. Mater.*, **26**(3), 362-391. https://doi.org/10.1016/S0079-6700(00)00046-0.

Sun, R., Fang, J., Goodwin, A., Lawther, J. and Bolton, A. (1998), "Isolation and characterization of polysaccharides from abaca fiber", *J. Agric. Food Chem.*, **46**(7), 2817-2822. https://pubs.acs.org/doi/abs/10.1021/jf9710894.

Tsai, W.T., Yang, J.M., Lai, C.W., Cheng, Y.H., Lin, C.C. and Yeh, C.W. (2006), "Characterization and adsorption properties of eggshells and eggshell membrane", *Bioresour. Technol.*, **97**(3), 488-493. https://doi.org/10.1016/j.biortech.2005.02.050.

Uddin, M.N., Li, L.Z., Ahmed, A. and Almajhali, K.Y.M. (2022), "Prediction of PVA fiber effect in Engineered Composite cement (ECC) by Artificial neural Network (ANN)", *Mater. Today Proc.*, **65**, 537-542. https://doi.org/10.1016/j.matpr.2022.03.088

Vasquez, J.Z. and Diaz, L.J.L. (2017), "Unidirectional abaca fiber reinforced thermoplastic starch composite", *Mater. Sci. Forum*, **894**, 56-61.

Vassilopoulos, A.P., Georgopoulos, E.F. and Dionysopoulos, V. (2007), "Artificial neural networks in spectrum fatigue life prediction of composite materials", *Int. J. Fatigue*, **29**(1), 20-29. https://doi.org/10.1016/j.ijfatigue.2006.03.004.

Vijaya Ramnath, B., Manickavasagam, V., Elanchezhian, C., Santhosh Shankar, A., Sundarrajan, R., Vickneshwaran, S. and Pithchai Pandian, S. (2014), "Investigation on flexural and impact properties of abaca and Manila hybrid composite", *Adv. Mater. Res.*, **1051**, 102-106. https://doi.org/10.4028/www.scientific.net/AMR.1051.102.

Vijayalakshmi, K., Neeraja, C.Y., Kavitha, A. and Hayavadana, J. (2014), "Abaca fibre", *Transact. Eng. Sci.*, **2**(9), 16-19.

Vilaseca, F., Valadez-Gonzalez, A., Herrera-Franco, P.J., Pèlach, M.À., López, J.P. and Mutjé, P. (2010), "Biocomposites from abaca strands and polypropylene, Part I: Evaluation of the tensile properties", *Bioresour. Technol.*, **101**(1), 387-395. https://doi.org/10.1016/j.biortech.2009.07.066.

Wang, X. and Zhang, L. (2021), "Physics-informed neural networks: A deep learning framework for solving the vibrational problems", *Adv. Nano Res.*, **11**(5), 495-519. https://doi.org/10.12989/anr.2021.11.5.495.

Wu, W., Cao, X., Zhang, Y. and He, G. (2013), "Polylactide /halloysite nanotube nanocomposites: Thermal, mechanical properties, and foam processing", *J. Appl. Polym. Sci.*, **130**(1), 443-452. https://doi.org/10.1002/app.39179.

Xu, Z., Chu, Z., Yan, L., Chen, H., Jia, H. and Tang, W. (2019), "Effect of chicken eggshell on the flame-retardant and smoke suppression properties of an epoxy-based traditional APP-PER-MEL system", *Polym. Compos.*, **40**(7), 2712-2723. https://doi.org/10.1002/pc.25077.

JL